



A long noncoding RNA at the cortex locus controls adaptive coloration in butterflies

Luca Livraghi^{a,b,1} , Joseph J. Hanly^{a,c,d} , Elizabeth Evans^e, Charlotte J. Wright^{b,f}, Ling S. Loh^a , Anyi Mazo-Vargas^{a,c} , Kiana Kamrava^a, Alexander Carter^a , Eva S. M. van der Heijden^{b,f} , Robert D. Reed^g , Riccardo Papa^{e,h,i,j} , Chris D. Jiggins^{b,1} , and Arnaud Martin^{a,1}

Affiliations are included on p. 8.

Edited by Sean Carroll, University of Maryland, College Park, MD; received February 16, 2024; accepted July 22, 2024

Evolutionary variation in the wing pigmentation of butterflies and moths offers striking examples of adaptation by crypsis and mimicry. The *cortex* locus has been independently mapped as the locus controlling color polymorphisms in 15 lepidopteran species, suggesting that it acts as a genomic hotspot for the diversification of wing patterns, but functional validation through protein-coding knockouts has proven difficult to obtain. Our study unveils the role of a long noncoding RNA (lncRNA) which we name *ivory*, transcribed from the *cortex* locus, in modulating color patterning in butterflies. Strikingly, *ivory* expression prefigures most melanic patterns during pupal development, suggesting an early developmental role in specifying scale identity. To test this, we generated CRISPR mosaic knock-outs in five nymphalid butterfly species and show that *ivory* mutagenesis yields transformations of dark pigmented scales into white or light-colored scales. Genotyping of *Vanessa cardui* germline mutants associates these phenotypes to small on-target deletions at the conserved first exon of *ivory*. In contrast, *cortex* germline mutant butterflies with confirmed null alleles lack any wing phenotype and exclude a color patterning role for this adjacent gene. Overall, these results show that a lncRNA gene acts as a master switch of color pattern specification and played key roles in the adaptive diversification of wing patterns in butterflies.

butterfly | lncRNA | evo-devo | pigmentation

The *cortex* locus represents a remarkable example of parallel evolution in butterflies and moths: the same genomic region has repeatedly evolved adaptive alleles that drive phenotypic variation within many diverse lineages. In particular, it underlies color variation involved in industrial melanism in geometrid moths *Biston*, *Phigalia*, and *Odontopera* (1, 2), forewing spots in the Bella Moth (3), adaptive mimicry in *Heliconius* butterflies (4–8) and *Papilio clytia* swallowtails (9), crypsis in leaf-mimicking *Kallima* butterflies (10), seasonal polyphenism in *Junonia* butterflies (11), female-limited melanism in *Pieris napi* (12), and pigmentation mutants in *Bombyx* silkworms (13).

Heliconius melpomene and *Heliconius erato* each exhibit intraspecific variation in their color patterns across the Neotropics. They also show spectacular examples of Müllerian mimicry, where multiple unpalatable species converge locally on a similar color pattern due to strong natural selection against visual predators and have evolved independent color patterning alleles at a handful of genetic loci (14). In naturally occurring *Heliconius* hybrid zones, association mapping has implicated discrete, modular noncoding intervals centered around *cortex*, suggesting differences in *cis*-regulatory elements (CREs) are the causal variants driving the presence–absence of hindwing yellow bars (5, 7, 15, 16). In a captive bred population of *H. melpomene*, a large spontaneous deletion line dubbed *ivory* (here named *ivory*^{Δ784}), yields butterflies with depigmented scales in the homozygous state, and involves a 78 kb structural variant that does not contain the protein coding region of *cortex* (17). To date, few hints as to how this locus modulates coloration have been gleaned. CRISPR knock-outs of *cortex* have resulted in rare, small clones with depigmented scale states (7, 11, 18). However, *cortex* is expressed in all epithelial and scale cell precursors of the butterfly wing during pupal development, seemingly with little correlation with adult color patterns (7), and its molecular function in meiosis-specific cell cycle regulation in *Drosophila* (19) makes it difficult to tie to pigmentation phenotypes. As such, whether *cortex* has a color patterning role remains an open question, and alternative mechanisms may be reconsidered. For example, prevailing genome annotations often neglect the presence of a class of noncoding transcripts, called long noncoding RNAs (lncRNAs), thus making them easy to miss during genotype–phenotype studies. While a majority of eukaryotic lncRNAs are considered to be transcriptional noise (20), a fraction of them have been described as genuine regulators of gene expression (21, 22). At the *cortex* locus, tiling arrays have revealed that color morphs of *H. melpomene* show differential transcription

Significance

Deciphering the genetic underpinnings of adaptive variation is fundamental for a comprehensive understanding of evolutionary processes. Long noncoding RNAs (lncRNAs) represent an emerging category of genetic modulators within the genome, yet they have been overlooked as a source of phenotypic diversity. In this study, we unveil the pivotal role of a lncRNA in orchestrating color transitions between dark and light patterns during butterfly wing development. Remarkably, this lncRNA gene is nested within the *cortex* locus, a genetic region known to control multiple cases of adaptive variation in butterflies and moths, including iconic examples of natural selection. These findings highlight the significant influence of lncRNAs in developmental regulation and underscore their potential as key genetic players in the evolutionary process itself.

The authors declare no competing interest.

This article is a PNAS Direct Submission.

Copyright © 2024 the Author(s). Published by PNAS. This article is distributed under Creative Commons Attribution-NonCommercial-NoDerivatives License 4.0 (CC BY-NC-ND).

¹To whom correspondence may be addressed. Email: miles.livraghi@gmail.com, c.jiggins@zoo.cam.ac.uk, or arnaud@gwu.edu.

This article contains supporting information online at <https://www.pnas.org/lookup/suppl/doi:10.1073/pnas.2403326121/-DCSupplemental>.

Published August 30, 2024.

of unannotated sequences (5), hinting at the presence of putative lncRNAs within the *ivory*^{Δ78k} interval. Nevertheless, assessing the role of lncRNAs in color patterning would require proper studies of their expression, function, and evolutionary conservation.

Here, the caveats and ambiguities about the role of *cortex* in scale fate specification motivated a closer examination of the genetic elements included in the *ivory* deletion in *Heliconius*, and by extension, of the mechanism behind the various phenotypes previously associated with the *cortex* locus. Parallel to a companion paper by Fandino et al. (23), we find in multiple species that a lncRNA encoding gene, that overlaps with the *ivory*^{Δ78k} deletion, is a potent modulator of melanic scale identities. As lncRNAs are being discovered and annotated at an increasing rate in genome databases, the range of their biological functions remain a broadly uncharted territory (21, 24). Importantly, the *ivory* lncRNA shows a conserved function in color scale specification, while having also evolved divergent expression patterns that precisely delineate pattern information in multiple species. We discuss how these findings not only join a rich literature on the emerging roles of lncRNA in development and gene regulation (25, 26) but also imply a direct role in the elaboration of adaptive phenotypic variation.

Results

A Previously Hidden Genetic Element Is Expressed at a Hotspot Locus.

Several color polymorphisms have been previously mapped to the *cortex* locus in both *H. melpomene* and *H. erato* (Fig. 1 A

and B) and are known to be under strong selection based on their participation in multispecies mimicry rings (27), narrow hybrid zones that reflect strong selection coefficients across ecological gradients (28, 29), and population genomics evidence of selective sweeps (30, 31). In *H. melpomene*, the causal alleles driving the presence–absence of yellow hindwing bars segregate into two regulatory regions, located 5' and 3' of *cortex*, that, respectively, control the ventral and dorsal wing surface (7, 16, 31). In *H. erato*, the same trait variation is controlled by distinct alleles mapping broadly over *cortex* or its 5' upstream region, respectively, specific to the Western Andes and to the Panama-Darién region (15, 30, 32).

To further explore the presence of genetic features in this genomic region, we reanalyzed RNA-seq data from pupal wings of *H. melpomene* and *H. erato* (39) and identified a polyadenylated, alternatively spliced lncRNA that is transcribed upstream of *cortex*, hereafter called *ivory* (SI Appendix, Figs. S1–S3). Both reference-based RNA-seq alignments and de novo transcriptome assemblies reveal that *ivory* encodes a ~1.3 kb transcript, containing up to eight exons spanning over 138 kb in *H. melpomene* and 205 kb in *H. erato* (Fig. 1B). Several exons appear to be TE derived but no sequence similarity to other regions in the genome exists. During the fifth instar larval wing development, *cortex* transcription initiates from a distal promoter, while *ivory* expression is absent (SI Appendix, Figs. S1 and S2). From 36 h after pupa formation, or ~20% of pupal development, *cortex* expression significantly decreases and *ivory* is detected and persists up until at least 60 h after pupa formation. In *H. erato*, we identified

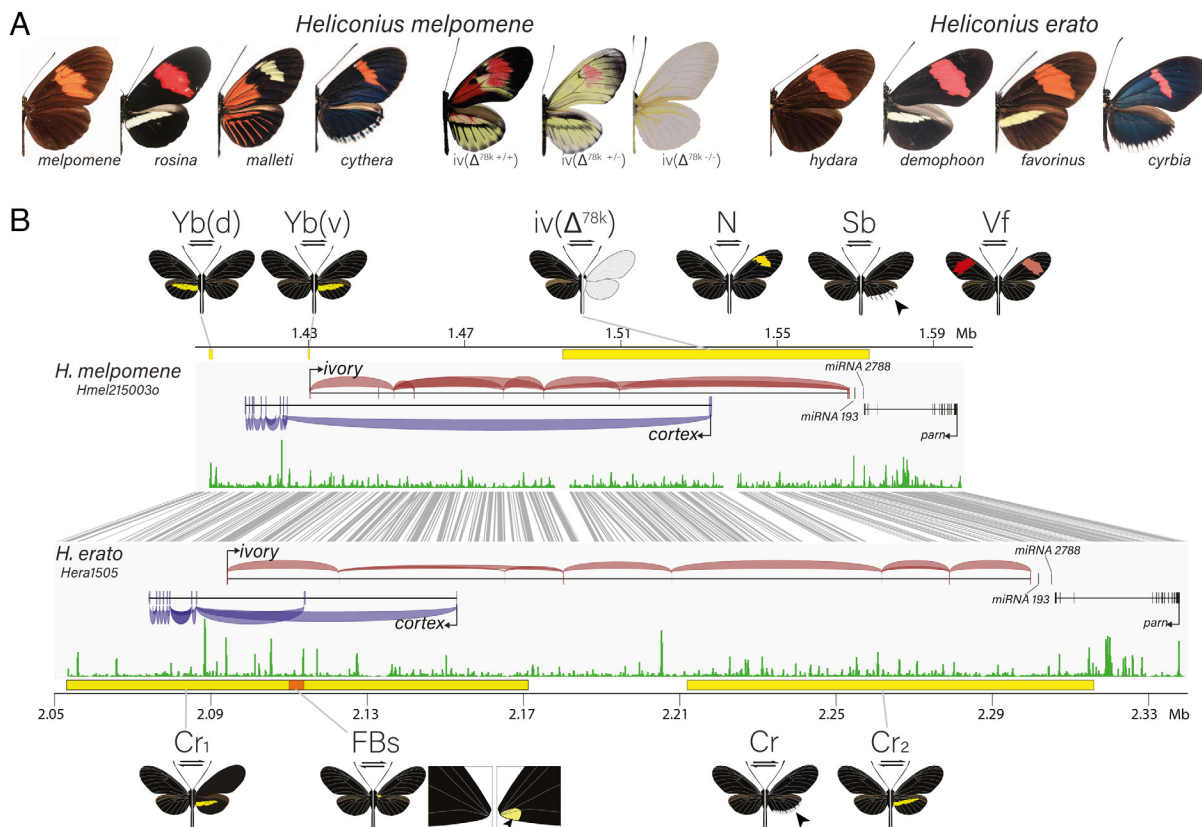


Fig. 1. Expression and CRISPR mKOs of the *ivory* lncRNA reveal color patterning roles. (A) Examples of *H. melpomene* and *H. erato* morphs exhibiting color pattern polymorphisms associated with the *cortex* locus, alongside representative phenotypes of the *ivory*^{Δ78k} deletion (17). (B) Summary of the association intervals previously mapped at the *cortex* locus for *H. melpomene* and *H. erato* (7, 15, 17, 30, 31). For *H. melpomene*: *Yb(d)* dorsal yellow bar (*Hmel2150030*: 1,403,500 to 1,405,500), *Yb(v)* ventral yellow bar (1,429,500 to 1,430,500), and *ivory*^{Δ78k} deletion (1,494,903 to 1,573,176). For *H. erato*: *Cr1* Peruvian (West of Andes) yellow bar (*Hera1505*: 2,053,037 to 2,171,230), *Cr2* Panamanian (East of Andes) yellow bar (2,211,881 to 2,315,926), and *FBS* forewing base spot (2110,000 to 2113,800). Current mapping intervals for *H. melpomene* loci *N*, *Sb*, and *Vf*, and the *H. erato* *Cr* locus are too large to indicate on the figure (33–36). Combined RNA-seq read junction events are shown for both *ivory* (red, positive strand) and *cortex* (blue, negative strand), with annotations for the adjacent *miRNAs* 193, 2788 (37) and for the gene *parn*. ATAC-seq tracks from normalized average read depth from 36 h pupal hindwings are shown in green (38). Gray lines indicate aligned regions >250 bp between *H. melpomene* and *H. erato*.

an additional lncRNA transcribed only in fifth instar caterpillars, sharing several antisense exons with *cortex* (SI Appendix, Fig. S1). In addition, ATAC-seq open-chromatin profiling from both species (38) showed that the *ivory* first exon is immediately 3' of a region of differential accessibility specific to pupal wing tissues, consistent with a promoter function (Fig. 1B and SI Appendix, Fig. S1).

The *ivory* lncRNA Is Necessary for Melanic Scale Development.

In order to investigate the potential functional roles of the *ivory* lncRNA, we next used CRISPR/Cas9 mutagenesis targeting the *ivory* promoter and first exon in order to test its putative function in wing patterning. These mosaic knock-outs, conducted in *H. erato*, *H. charithonia*, and *Vanessa cardui*, generated butterflies with pronounced shifts in pigmentation, consisting of scale transformations from melanic to yellow-white states (Fig. 2 and SI Appendix, Figs. S4 and S5), phenocopying the effects of the *ivory*^{Δ78k} mutant in *H. melpomene* (17). The high penetrance of this phenotype (in 57% of adults), as well as the large size of

mutant clones, often spanning entire individuals that emerged healthily (Fig. 2 and SI Appendix, Tables S1 and S2), suggests a low pleiotropy of the *ivory* CRISPR phenotypes, with no detectable effects other than in epithelial scales throughout the adult wing and body. Moreover, in situ hybridizations against the first exon of *ivory* showed that the *ivory* lncRNA is expressed in perfect correlation with melanic scales during pupal wing development, including for two *H. erato* morphs that differ in the presence-absence of the yellow hindwing bar. This association was previously not found for the *cortex* mRNA or protein (7). Together, these data strongly suggest that *ivory* is the causative locus generating pattern divergence in nymphalid butterflies, rather than *cortex* as previously thought (5, 7, 10).

Phenotypic Effects are Specific to the *ivory* lncRNA. CRISPR-induced mutant clones may include deletions that are larger than intended, particularly in G₀-injected individuals, where such effects are difficult to genotype. To overcome the limitations of mosaic knock-outs, we thus sought to generate *ivory* KO lines



Fig. 2. Expression of *ivory* associates with melanic scales in nymphalid butterflies. (A–C) Expression of *ivory* in 30% pupal wing tissue of *H. erato* prefigures adult melanic scales, and mKO results in a complete loss of black scales. Unbanded morphs of *H. erato* express *ivory* in the presumptive yellow bar region (white arrowheads). Expression is absent in presumptive red (D–D') and yellow (E–E') regions in the banded morph. (F–J') Expression and function are conserved in *H. charithonia*, strongly marking future black scales, resulting in yellow/white states in the mKOs. (K–M) Function is conserved outside *Heliconius*, with *V. cardui* displaying similar loss of melanic scales in the mKOs and a strong correlation between *ivory* expression and adult black patterns. (N–N'') Expression of *ivory* is absent from ventral forewing orange-red ommochrome scales, as well as from (O–O') white margin patterns and yellow eyespot rings.

in the Painted Lady butterfly *V. cardui*, a species amenable to mass-rearing in laboratory conditions. We generated G₁ and G₂ *V. cardui* *ivory* mutants by crossing G₀ individuals displaying mosaic *ivory* mutations, followed by G₁ pooled matings. This generated viable mutants displaying marked reductions of melanin on all scales, including in the thorax, head, abdomen, and antennae (Fig. 3 D–F and *SI Appendix*, Figs. S5 and S6). Tyrosine and Tryptophan radiolabeling experiments—melanin and ommochrome precursors, respectively—indicate a strong correspondence between *ivory* KOs and melanin-containing scales (Fig. 3 D and E and *SI Appendix*, Figs. S7–S9). Whole-genome sequencing of G₁ and G₂ individuals revealed that compound heterozygosity at the targeted site, typically consisting of two deletion alleles of unequal size, was associated with *ivory* phenotypes of variable expressivity (*SI Appendix*, Fig. S10). For example, we established that a biallelic deletion spanning 82/97 bp across the lncRNA first exon is sufficient to generate a strong *ivory* phenotype (Fig. 3F). These associations between *ivory* exonic deletions and the coloration phenotype, together with the spatial expression of the lncRNA in association with the affected patterns, show that expression of the *ivory* lncRNA

positively regulates melanic scale differentiation during pupal wing development.

Germline Mutants of *Cortex* Rule Out a Color Patterning Function. Previous knock-outs of *cortex* exons generated rare phenotypes in mosaic G₀ butterflies (7, 10, 11). To circumvent the limitations of mosaic KOs and formally test a function of *cortex*, we generated *V. cardui* null mutants targeting the second exon of *cortex*, an obligatory exon shared between all larval and pupal isoforms in *Heliconius* (*SI Appendix*, Figs. S1 and S2; ref. 5) and that includes a conserved C-Box motif crucial for APC/C interaction (7). The resulting *cortex* crisprants were indistinguishable from wild-type controls, in spite of high mutation rates observed in the genotyped haemolymph of 7 G₀ individuals (*SI Appendix*, Fig. S11). We next crossed two confirmed G₀ mutants (Fig. 3 G and G') and produced F₁ individuals, again displaying no pigmentation changes on their wings (Fig. 3 I and I'). We recovered several compound heterozygous mutants, harboring two null alleles with premature stop codons, resulting in the early truncation of the *cortex* protein and a complete loss of secondary structure (Fig. 3 J and K and *SI Appendix*, Fig. S12). *Cortex* biallelic mutants were viable, but

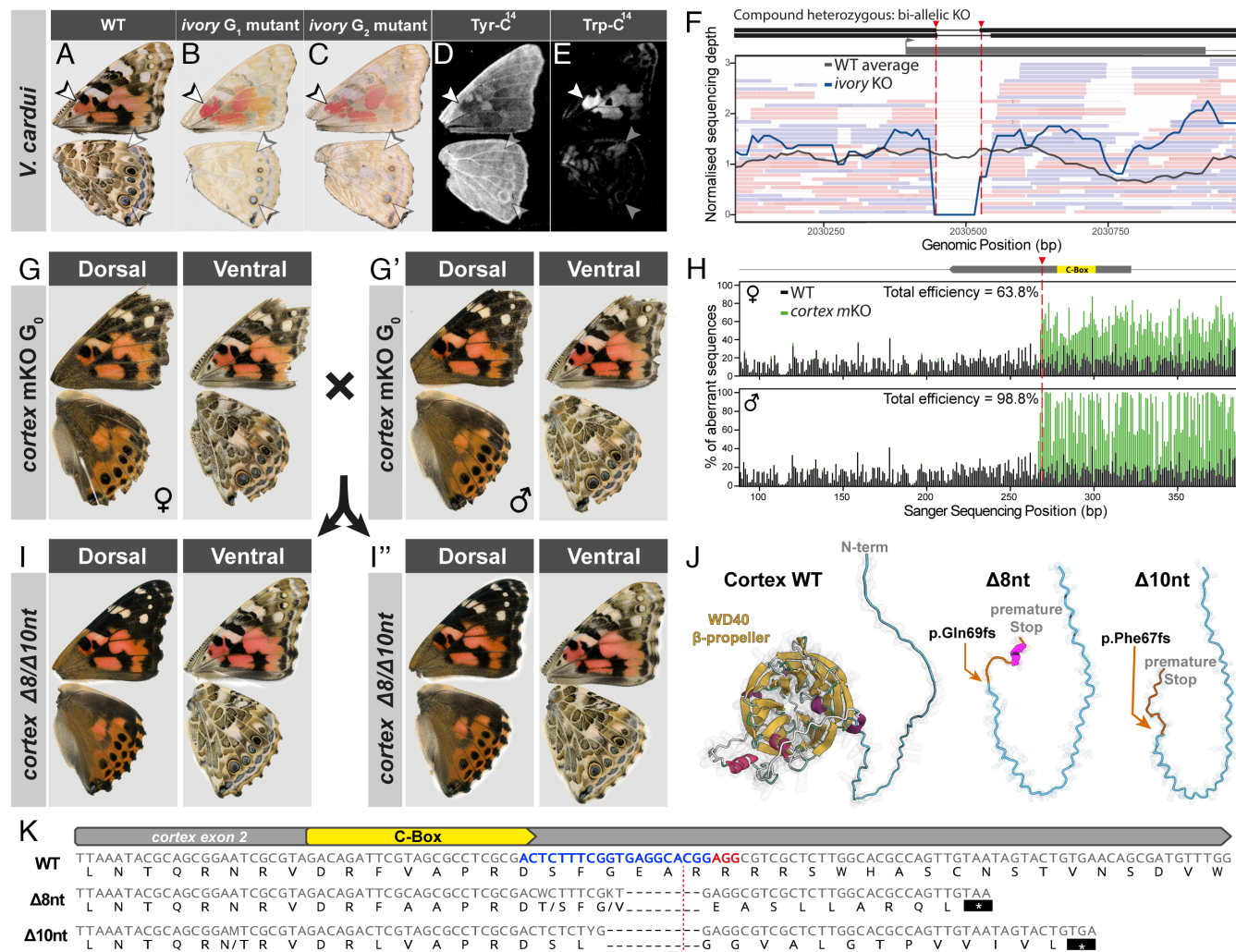


Fig. 3. Phenotypes are explained by *ivory*-specific mutations. (A–C) Loss of melanic scales in *ivory* germline mutants. (D) Radiolabeling of Tyrosine highlighting melanin containing scales and (E) Tryptophan radiolabeling revealing the distribution of ommochrome-containing patterns. Ommochromes are not affected by *ivory* KOs in *V. cardui* (arrowheads). (F) Strong *ivory* phenotype shown in (B) is explained by a compound heterozygous deletion of 82/97 bp at its first exon. (G and H) Exon 2 G₀ *cortex* crisprants display no wing phenotypes, but a large fraction of cells carrying mutations at the expected cut site. These crisprants were crossed to produce F₁ offspring (I and I'), again displaying no wing phenotypes. (I and K) Genotyped alleles recovered in the F₁ lead to premature protein truncation due to an 8 nt and 10 nt deletion at *cortex* exon 2. Panel J, yellow: predicted Beta-sheet structures; magenta: predicted alpha-helices; orange: frame-shifted amino acid residues. Panel K, blue: sgRNA sequence; red: protospacer adjacent motif; dotted line: predicted CRISPR cutting site.

infertile, consistent with a meiosis-specific role of *Cortex* in *Drosophila* (40). Together, these results rule out a function for *cortex* in *V. cardui* wing scale pigmentation.

Importantly, the lack of a *cortex* wing patterning function suggests that *ivory* does not have a local *trans*-regulatory effect on its neighboring gene and that the *ivory* promoter is not acting in *cis* to regulate *cortex*. To further examine potential local *cis*-acting targets, we reanalyzed Hi-C and histone ChIP-seq data previously generated in *H. erato* pupal wings (41, 42). Chromatin conformation capture assays detect a strong topologically associated domain (TAD) centered around *ivory* (SI Appendix, Fig. S13), with no evidence of long-range interactions outside of this domain. Furthermore, histone modification profiling performed in three-day-old pupal wings reveals that the *ivory* 5' region coincides with a strong H3K4me3 signal, a hallmark of transcriptionally active promoters (43, 44). Given the absence of other protein-coding genes within the TAD other than *cortex*, and a chromatin state consistent with a promoter rather than enhancer activity, it is likely that *ivory* is acting in *trans* and not through *cis*-regulation of nearby genes.

A Conserved Function for *Ivory* in Nymphalid Butterflies. The sequence conservation of lncRNAs is often limited to 5' ends of transcripts and degrades rapidly over evolutionary time (45). We identified the *ivory* promoter and first exon as conserved in ditrysian Lepidoptera (SI Appendix, Fig. S14), which enabled the expression profiling and CRISPR mutagenesis of a homologous region in a further two nymphalid butterflies spanning ~80 million years of evolution (46). CRISPR/Cas9 targeting of *ivory* in *Agraulis incarnata* and *Danaus plexippus* resulted in crisprants displaying scale transformations from melanic to yellow-white states, as well as lighter orange colors (Fig. 4).

In *A. incarnata*, *ivory* mKOs resulted in scale transformations from melanic to reflective white/silver scales (Fig. 4 A–C and SI Appendix, Fig. S16). Closer inspection through scanning electron microscopy revealed that these transformed scales not only underwent a loss of melanin pigmentation but also a change in the ultrastructure of their top surface (SI Appendix, Fig. S17), showing an ectopic lamination characteristic of reflective scale types (47). While a subset of dorsal melanic spots only showed a lighter intensity in *ivory*-deficient clones (Fig. 4 G, I, and I'), others showed complete conversion to white, such as the marginal patterns and venous black markings (Fig. 4 J and J'). Orange patterns showed a lighter coloration in crispant clones, likely due to a reduction in melanin content, but consistent with a model where these patterns also incorporate ommochrome pigments that are unaffected in *ivory* mKOs (SI Appendix, Fig. S16).

In *D. plexippus* *ivory* crisprants, melanic scales again turned white, and orange scales also appeared lighter, an effect especially pronounced on ventral wing surfaces (Fig. 4 K–M). Interestingly, distal white spots on the ventral forewings changed from white to orange, while more distal orange areas showed the opposite effect, turning from orange to white, indicating that there are local differences in *ivory* function (Fig. 4 N and N'). These effects were consistent on both wing surfaces in *D. plexippus* (Fig. 4 P–R), with pronounced melanic-to-white transformations around the vein margins in both forewings (Fig. 4 S and S') and hindwings (Fig. 4 T and T').

Discussion

Cortex—A Case of Mistaken Identity? Color variation loci in peppered moths and *Heliconius* butterflies include the protein coding gene *cortex*, which was originally proposed as a causal gene

within the corresponding genetic intervals based on its differential expression profile (1, 5). Several follow-up studies used CRISPR to mutagenize a coding exon of *cortex* and generated crisprants with discolored clones in *Heliconius*, *Danaus*, *Junonia*, and *Kallima* butterflies (7, 10, 11), further anchoring the incorrect impression that *cortex* itself is necessary for color specification during development. In parallel with findings in *Junonia coenia* and *Bicyclus anynana* (23, 48), we show that a lncRNA gene adjacent to *cortex* is in fact controlling wing pigmentation.

This misidentification was caused by two main issues. First, *ivory* had escaped detection as it was missing from former genome annotations. This is likely the consequence of the erroneous exclusion of noncoding transcripts by genome annotation pipelines and is reflective of a general bias toward protein coding genes in our understanding of development and evolution. Second, CRISPR repair events occasionally create deletion alleles that are much larger than intended (49–54). We also recovered large deletions in the 10 kb to 30 kb range in a batch of *G*₁ siblings following CRISPR targeting (SI Appendix, Supporting Text and Fig. S18). Assuming that CRISPR-induced structural variants occur at low frequency, we suggest that sporadic, large deletions induced by *cortex* mutagenesis fortuitously reached *ivory*, explaining the low penetrance of wing phenotypes in these previous experiments. The differential expression of *cortex* in fifth instar larval wing discs is therefore independent of scale melanization roles and may reflect a highly dynamic temporal expression typical of cell cycling genes. It thus appears unlikely that *cortex* modulates pigment variation in other butterflies and moths. Instead, the *ivory* lncRNA, which is partly nested within the *cortex* gene, is a proven regulator of color scale specification and the likely causal driver of pattern variation in natural populations.

A lncRNA Repeatedly Drives Adaptive Phenotypic Variation. There has been considerable interest in the *cortex/ivory* region, as it was independently mapped as the master switch locus behind striking examples of adaptive variation, namely industrial melanism in peppered moths (1, 2), Müllerian mimicry in *Heliconius* (4–8), Batesian mimicry in *P. clyta* (9), seasonal polyphenism in *Junonia* (11), and leaf-mimicking crypsis in oakleaf butterflies (10). Adaptive variation between morphs consists of shifts in the intensity and spatial distribution of melanin-containing scales in all of these cases. In our study, we showed that *ivory* expression consistently prefigured the distribution of melanic scales in nymphalid butterflies and that in fact *ivory* and not *cortex* is required for their specification.

This stimulates a reframing of previous population genetics studies. We now infer that regulatory alleles of *ivory* drive the repeated evolution of pattern variation involving a shift between black and white/yellow. Indeed, *H. melpomene* and *H. erato* comimics geographically vary in the display of their hindwing yellow-band and marginal white-spots across their range. These polymorphisms map to modular noncoding regions of the *cortex-ivory* locus (Fig. 1B), that independently control melanism over the ventral and dorsal hindwing yellow bars, and the white hindwing marginal regions (5, 7, 15, 30, 32, 55). As *ivory* controls melanic pattern distribution in *Heliconius* (Fig. 2 A and B), these population genomic signals likely point at CREs that switch *ivory* expression on or off at these color patterns. Supporting this idea, we show that a morph of *H. erato* that lacks a hindwing yellow bar expresses *ivory* throughout this region (Fig. 2 A–C), consistent with the dominance of black over yellow in hybrid crosses (32, 35). Indeed, our previous study identified what we now believe is likely a yellow-bar-specific enhancer of *ivory* (rather than *cortex*) which drives its expression in a yellow-bar-specific pattern (SI Appendix, Fig. S19) (7).



Fig. 4. Conserved and pattern-specific effects of *ivory* mKOs on nymphalid butterflies. Wing pattern effects of *ivory* perturbation in representative *A. incarnata* and *D. plexippus* G_0 crispants. (A–E') Ventral wing views of *A. incarnata* comparing wild-type to full (nonmosaic) *ivory* crispant and a clonal *ivory* crispant (i.e., with fragmented mosaic of WT and mutant clones). Phenotypes include melanic (black/brown)-to-silver transformations and lighter orange (dashed lines). Insets feature magnified views of the Cu_1 – Cu_2 silver spots in forewings (D and D'), and hindwings (E and E'). (F–J') Dorsal views, featuring *ivory* crispant clones with lightened orange and black coloration (F and F', Discalis II spots), and melanic-to-white conversions (F and F', marginal M_3 – Cu_2 region). (K–O') Ventral wing views of *D. plexippus* comparing wild-type to full and clonal *ivory* crispants. Insets feature the forewing M_1 – M_3 white spot region (N and N') and the hindwing discal crossvein (O and O'), with conversions of both melanic and orange to white states, as well as a residual orange coloration in some of the affected areas. (P–T') Dorsal views, with insets featuring the forewing Cu_1 – Cu_2 vein junction (S and S') and the hindwing M_1 – M_2 vein junctions (T and T').

Likewise, in *Heliconius numata* and *Kallima inachus*, adaptive color morphs have been linked to inversion polymorphisms, allowing complex regulatory haplotypes to accumulate in the absence of recombination (8, 10, 56). This mechanism likely underlies the

fine-tuning of *ivory* expression, and while a role of other genes within these inversions is not excluded (i.e., a supergene), *ivory* likely explains a large fraction of the color pattern variations that are involved in Müllerian and leaf mimicry in these species.

The *ivory* lncRNA Acts Primarily on Melanic Scale Identities. The expression of *ivory* prefigures the position of melanic patterns at a stage where known master selector genes define scale identity (14), and perturbation of *ivory* resulted in the transformation of melanic scales into white or light-colored identities. These scale color shifts were observed both on the wings and body. Melanic scales contain either NBAD-melanin or DOPA-melanin pigments; two end-products of the insect melanin synthesis pathway following the metabolism of Tyrosine into dopamine pigment precursors (57, 58). Lighter colored scales may contain the dopamine by-product NADA-sclerotin, a clear molecule that cross-links cuticular proteins and participates in scale hardening (59, 60). Our working model thus posits that *ivory* activates melanic color outputs by indirectly promoting dopamine–melanin synthesis or by antagonizing the production of NADA-sclerotin, explaining the predominance of white scales in *ivory* knock-outs. Modulating the ratio of dopamine–melanin and NADA-sclerotin may also explain the ultrastructural increase in the upper lamina of *ivory*-deficient scales (*SI Appendix*, Fig. S17), since similar effects on scale upper laminae occur in *Bicyclus* mutants with reduced dopamine–melanin (57). Of note, some areas in *A. incarnata* and *V. cardui* crispants showed partial phenotypes, with orange patterns showing a lighter coloration in mutant clones. This effect is likely explained by a mix of pigment in these scales, supported by radiolabeling experiments (*SI Appendix*, Figs. S7–S9 and S16). These data suggest that while nymphalid color patterns can consist of discrete melanic and ommochrome identities, some scales can also contain mixtures of both pigment types.

Ivory crispant clones also showed a light-yellow pigmentation in *H. erato* and *H. charithonia* (*SI Appendix*, Figs. S8 and S9), which is attributed to 3-hydroxykynurenine (3-OHK), a yellow Trp-derived pigment that is incorporated into yellow *Heliconius* scales from circulating hemolymph during late pupal development and not into black scales (61–63). We thus conclude that *ivory* acts to prevent 3-OHK incorporation into melanic scales (*SI Appendix*, Fig. S9 D–F). Finally, we also note that some *H. erato* *ivory* mutants showed effects on red color pattern elements, with paler red scales on dorsal forewings, and a complete loss of red pigments on ventral forewings (*SI Appendix*, Fig. S8). Unlike pigmented scales that incorporated 3-OHK, *H. erato* red scales synthesize ommochrome pigments from incorporated Trp (63). These phenotypes suggest that *ivory* may be necessary for the normal production of ommochromes in this species, as also inferred in *J. coenia* (23), but not in *V. cardui* or *A. incarnata* where pink, red, and orange persisted in *ivory* crispants (see above). Taken together, these results suggest that *ivory* acts as an upstream regulatory factor that can orchestrate several aspects of scale pigmentation, promoting dark melanin metabolism and also regulating some aspects of ommochrome pigmentation pathways in some species.

ivory Controls Melanic Fates Via *Trans*-Regulatory Mechanisms.

The precise molecular mechanism by which *ivory* controls pigmentation is as of yet unclear, but is gaining clarity. Here, we have shown it is not acting in *cis* to regulate the adjacent *cortex* gene and that chromatin conformation and histone modification at the *ivory* promoter is inconsistent with a distal enhancer role function (*SI Appendix*, Fig. S13). Deletion of *ivory* in *J. coenia* results in overexpression of *mamo*, a transcription factor gene known to act as a repressor of dark melanic states (64). It follows that *ivory* acts in *trans* to regulate other genes. Remarkably, a parallel study showed that short deletions in the *miR-193* gene of *B. anynana* butterflies produces pigmentation defects analogous to the *ivory* KO effects we described (48). This miRNA is situated immediately downstream (3') of the *ivory* transcripts we have detected in

H. erato and *V. cardui*. This leads to a model where the *ivory* lncRNA would belong to a class of noncoding precursor transcript (lnc-pri-miRNA) from which miRNAs are excised before further processing (65). This mechanism is compatible with lncRNA annotations being disjuncted from the miRNA units (Fig. 1B), because miRNA excision occurs immediately during transcriptional elongation (65). As the second miRNA at this locus (*miR2788*) did not show coloration phenotypes when mutagenized in this study, *miR193* could be the sole *trans*-acting factor regulating the pigment specification program, or alternatively, it could act in unison with the *ivory* processed lncRNA (66). Further work is needed to identify the direct regulatory interactions that mediate *ivory*/*miR193* expression to the spectacular effects on coloration mediated by this noncoding locus.

Conclusion

Only a few lncRNA genes have been linked to adaptive variation in natural populations, including a locus-producing phased siRNAs that modulate monkeyflower coloration, and a nuclear RNA involved in thermal adaptation in fruit flies (67, 68). In this study, we showed that the *ivory* lncRNA is spatially regulated during development and is required for melanic scale identity. Remarkably, this role is conserved in nymphalid butterflies across 80 MY of divergence (46) and includes cases where allelic variation at the *ivory* locus itself drives phenotypic adaptations, such as the yellow band vs. melanic pattern switches involved in *Heliconius* mimicry. Future characterization of *ivory* alleles in polymorphic populations of butterflies, as well as in geometrid moths that underwent episodes of industrial melanism (2), promises to be an exciting avenue of research on the molecular basis of adaptation. More generally, our findings further establish that lncRNAs are not only important regulators of development but also pivotal drivers of evolutionary change at the genetic level.

Methods

Butterfly Rearing. *H. erato demophoon* (banded morph), *H. erato hydara* (unbanded morph), *H. melpomene rosina* (origin: Panama), and *H. charithonia charithonia* (origin: Puerto Rico) were reared in greenhouse environments using primarily *Passiflora biflora* as a host plant, as well as *Passiflora menispermifolia* and *Passiflora vitifolia* for *H. melpomene* (7). *A. incarnata* were reared at 25 °C or 28 °C on *P. biflora*, *Passiflora caerulea*, *Passiflora incarnata* or an artificial diet (passionvine butterfly diet, Monarch Watch Boutique, supplemented with 30 g/L of water of fine ground *P. biflora* leaf powder). *A. incarnata* adults were kept in a greenhouse cage with nectaring sources (*Gatorade* 50% in feeding cups, *Lantana camara*, *Buddleja davidii*) and supplemented with UV-light (Repti-Glo 10.0 Compact Fluorescent Desert Terrarium Lamp bulbs, Exo Terra). *V. cardui* (stock origin: Carolina Biological Supplies) were reared on an artificial diet with oviposition on *Alcea rosea* or *Malva sylvestris*. *D. plexippus* were reared on *Asclepias curassavica* in greenhouse conditions.

De Novo Transcriptome Assemblies. Raw RNA-seq data reads were obtained from Bioproject PRJNA552081 (39) and used to generate de novo transcriptome assemblies for *H. erato demophoon*, *H. erato hydara*, *H. melpomene melpomene*, and *H. melpomene rosina* (*SI Appendix*, Table S1) (69). Transcriptome assemblies were generated using Trinity v2.10.0 with a minimum length of 200 bp and the default K-mer of 25 (70). Residual adapters present in the assembly were trimmed using FCS adaptor (71) and contigs less than 200 bp in length were removed.

CRISPR Mosaic Knock-outs (mKOs). Butterfly embryo microinjections followed published procedures (7) using 1:1 or 2:1 mass ratios of Cas9-2xNLS (PNABio or QB3 Macrolabs) and synthetic sgRNAs (Synthevo, listed in *SI Appendix*, Table S3). Injections were completed before blastoderm formation around 4 h (*SI Appendix*, Table S1), most of them within 2 h AEL, thus preceding the first mitotic cleavage (72, 73). Survival

and phenotypic penetrance were assessed in neonates, pupae, and adults, and no morphological phenotypes were visible in immatures in this study.

In Situ Hybridizations. Chromogenic RNA *in-situ* hybridization (ISH) followed previously described procedures (74) with the following modifications. Antisense riboprobes targeting the conserved *ivory* first exon of each species were transcribed from PCR templates that were amplified from wing cDNA and gDNA (*SI Appendix, Table S4*). Developing wings were dissected at 20 to 35% pupal development, incubated in fixative for 30 to 40 min (1X PBS, 2 mM egtazic acid, 9.25% formaldehyde), and stored in MeOH at -20 °C. On the day of the hybridization procedure, wings were rehydrated progressively in PBT (1X PBS, 0.1% Tween20) and digested with 2.5 µg/mL Proteinase K for 5 min on ice before postfixation and hybridization with 40 ng/µL of DIG-labeled riboprobe at 60 to 63 °C. Wings were stained at room temperature for 4 to 6 h in BM Purple (Roche Applied Science).

Data, Materials, and Software Availability. Whole-genome sequencing data are available in the Sequence Read Archive (75) (www.ncbi.nlm.nih.gov/sra) under BioProject accession numbers [PRJNA1031670](https://www.ncbi.nlm.nih.gov/bioproject/PRJNA1031670). Trinity assemblies have been deposited on the Open Science Framework repository (69).

1. A. E. Van't Hof, *et al.*, The industrial melanism mutation in British peppered moths is a transposable element. *Nature* **534**, 102–105 (2016).
2. A. E. Van't Hof, L. A. Reynolds, C. J. Yung, L. M. Cook, I. J. Saccheri, Genetic convergence of industrial melanism in three geometrid moths. *Biol. Lett.* **15**, 20190582 (2019).
3. J. Zhang *et al.*, What one genus of showy moths can say about migration, adaptation, and wing pattern. *Proc. Natl. Acad. Sci. U.S.A.* **121**, e2319726121 (2024).
4. B. Huber *et al.*, Conservatism and novelty in the genetic architecture of adaptation in *Heliconius* butterflies. *Heredity* **114**, 515–524 (2015).
5. N. J. Nadeau *et al.*, The gene cortex controls mimicry and crypsis in butterflies and moths. *Nature* **534**, 106–110 (2016).
6. S. V. Saenko *et al.*, Unravelling the genes forming the wing pattern supergene in the polymorphic butterfly *Heliconius numata*. *EvoDevo* **10**, 1–12 (2019).
7. L. Livraghi *et al.*, Cortex cis-regulatory switches establish scale colour identity and pattern diversity in *Heliconius*. *eLife* **10**, e68549 (2021).
8. H. Bastide, S. V. Saenko, M. Chouteau, M. Joron, V. Llaurens, Dominance mechanisms in supergene alleles controlling butterfly wing pattern variation: Insights from gene expression in *Heliconius numata*. *Heredity* **130**, 92–98 (2023).
9. N. W. VanKuren, D. Massardo, S. Nallu, M. R. Kronforst, Butterfly mimicry polymorphisms highlight phylogenetic limits of gene reuse in the evolution of diverse adaptations. *Mol. Biol. Evol.* **36**, 2842–2853 (2019).
10. S. Wang *et al.*, The evolution and diversification of oakleaf butterflies. *Cell* **185**, 3138–3152 (2022).
11. K. R. van der Burg *et al.*, Genomic architecture of a genetically assimilated seasonal color pattern. *Science* **370**, 721–725 (2020).
12. K. Tunström *et al.*, The genetic basis of a regionally isolated sexual dimorphism involves cortex (2024).
13. K. Ito *et al.*, Mapping and recombination analysis of two moth colour mutations, Black moth and Wild wing spot, in the silkworm *Bombyx mori*. *Heredity* **116**, 52–59 (2016).
14. W. O. McMillan, L. Livraghi, C. Concha, J. J. Hanly, From patterning genes to process: Unraveling the gene regulatory networks that pattern *Heliconius* wings. *Front. Ecol. Evol.* **8**, 221 (2020).
15. S. M. Van Belleghem *et al.*, Complex modular architecture around a simple toolkit of wing pattern genes. *Nat. Ecol. Evol.* **1**, 52 (2017).
16. J. Enciso-Romero *et al.*, Evolution of novel mimicry rings facilitated by adaptive introgression in tropical butterflies. *Mol. Ecol.* **26**, 5160–5172 (2017).
17. J. J. Hanly *et al.*, A large deletion at the cortex locus eliminates butterfly wing patterning. *G3* **12**, jkac021 (2022).
18. S. Wang *et al.*, The evolution and diversification of oakleaf butterflies. *Cell* **185**, 3138–3152 (2022).
19. J. A. Pesin, T. L. Orr-Weaver, Developmental role and regulation of cortex, a meiosis-specific anaphase-promoting complex/cyclosome activator. *PLoS Genetics* **3**, e202 (2007).
20. R. Ard, R. C. Allshire, S. Marquardt, Emerging properties and functional consequences of noncoding transcription. *Genetics* **207**, 357–367 (2017).
21. J. S. Mattick *et al.*, Long non-coding RNAs: Definitions, functions, challenges and recommendations. *Nat. Rev. Mol. Cell Biol.* **24**, 430–447 (2023).
22. C.-C. Hon *et al.*, An atlas of human long non-coding RNAs with accurate 5' ends. *Nature* **543**, 199–204 (2017).
23. R. A. fandino *et al.*, The ivory lncRNA regulates seasonal color patterns in buckeye butterflies. *bioRxiv* [Preprint] (2024). Available at: <https://www.biorxiv.org/content/10.1101/2024.02.09.597733v1>. Accessed 13 February 2024.
24. C. P. Ponting, W. Haerty, Genome-wide analysis of human long noncoding RNAs: A provocative review. *Annu. Rev. Genom. Hum. Genet.* **23**, 153–172 (2022).
25. K. N. Smith, S. C. Miller, G. Varani, J. M. Calabrese, T. Magnuson, Multimodal long noncoding RNA interaction networks: Control panels for cell fate specification. *Genetics* **213**, 1093–1110 (2019).
26. A. Mangiavacchi, G. Morelli, V. Orlando, Behind the scenes: How RNA orchestrates the epigenetic regulation of gene expression. *Front. Cell Dev. Biol.* **11**, 1123975 (2023).
27. Heliconius Genome Consortium, Butterfly genome reveals promiscuous exchange of mimicry adaptations among species. *Nature* **487**, 94–98 (2012).
28. N. Rosser, K. K. Dasmahapatra, J. Mallet, Stable *Heliconius* butterfly hybrid zones are correlated with a local rainfall peak at the edge of the Amazon basin. *Evolution* **68**, 3470–3484 (2014), 10.1111/evo.12539.
29. S. M. Van Belleghem *et al.*, Selection and isolation define a heterogeneous divergence landscape between hybridizing *Heliconius* butterflies. *Evolution* **75**, 2251–2268 (2021).
30. M. Moest *et al.*, Selective sweeps on novel and introgressed variation shape mimicry loci in a butterfly adaptive radiation. *PLoS Biol.* **18**, e3000597 (2020).
31. J. I. Meier *et al.*, Haplotype tagging reveals parallel formation of hybrid races in two butterfly species. *Proc. Natl. Acad. Sci. U.S.A.* **118**, e2015005118 (2021).
32. L. S. Maroja, R. Alschuler, W. O. McMillan, C. D. Jiggins, Partial complementarity of the mimetic yellow bar phenotype in *Heliconius* butterflies. *PLoS one* **7**, e48627 (2012).
33. P. M. Sheppard, J. R. G. Turner, K. S. Brown, W. W. Benson, M. C. Singer, Genetics and the evolution of muellerian mimicry in *heliconius* butterflies. *Philos. Trans. R Soc. Lond Series B-Biol. Sci.* **308**, 433 (1985).
34. R. E. Naisbit, C. D. Jiggins, J. Mallet, Mimicry: Developmental genes that contribute to speciation. *Evol. Dev.* **5**, 269–280 (2003).
35. M. Joron *et al.*, A conserved supergene locus controls colour pattern diversity in *Heliconius* butterflies. *PLoS Biol.* **4**, 1831–1840 (2006).
36. L. Ferguson *et al.*, Characterization of a hotspot for mimicry: Assembly of a butterfly wing transcriptome to genomic sequence at the *HmYb/Sb* locus. *Mol. Ecol.* **19**, 240–254 (2010).
37. A. K. Surridge *et al.*, Characterisation and expression of microRNAs in developing wings of the neotropical butterfly *Heliconius melpomene*. *BMC Genomics* **12**, 62 (2011).
38. S. M. Van Belleghem *et al.*, High level of novelty under the hood of convergent evolution. *Science* **379**, 1043–1049 (2023).
39. J. J. Hanly, R. W. Wallbank, W. O. McMillan, C. D. Jiggins, Conservation and flexibility in the gene regulatory landscape of heliconiine butterfly wings. *EvoDevo* **10**, 1–14 (2019).
40. T. Chu, G. Henrion, V. Haegeli, S. Strickland, Cortex, a *Drosophila* gene required to complete oocyte meiosis, is a member of the *Cdc20/fizzy* protein family. *Genesis* **29**, 141–152 (2001).
41. J. J. Lewis, R. D. Reed, Genome-wide regulatory adaptation shapes population-level genomic landscapes in *Heliconius*. *Mol. Biol. Evol.* **36**, 159–173 (2018).
42. J. J. Lewis *et al.*, Parallel evolution of ancient, pleiotropic enhancers underlies butterfly wing pattern mimicry. *Proc. Natl. Acad. Sci. U.S.A.* **116**, 24174–24183 (2019).
43. P. V. Kharchenko *et al.*, Comprehensive analysis of the chromatin landscape in *Drosophila melanogaster*. *Nature* **471**, 480–485 (2011).
44. L. A. Gates, C. E. Foulds, B. W. O'Malley, Histone marks in the 'drivers seat': Functional roles in steering the transcription cycle. *Trends Biochem. Sci.* **42**, 977–989 (2017).
45. H. Hezroni *et al.*, Principles of long noncoding RNA evolution derived from direct comparison of transcriptomes in 17 species. *Cell Rep.* **11**, 1110–1122 (2015).
46. A. Y. Kawahara *et al.*, A global phylogeny of butterflies reveals their evolutionary history, ancestral hosts and biogeographic origins. *Nat. Ecol. Evol.* **7**, 903–913 (2023).
47. A. Ren *et al.*, Convergent evolution of broadband reflectors underlies metallic coloration in butterflies. *Front. Ecol. Evol.* **8**, 206 (2020).
48. S. Tian *et al.*, A micro-RNA drives a 100-million-year adaptive evolution of melanic patterns in butterflies and moths. *bioRxiv* [Preprint] (2024). Available at: <https://www.biorxiv.org/content/10.1101/2024.02.09.597741v1>. Accessed 13 February 2024.
49. H. Y. Shin *et al.*, CRISPR/Cas9 targeting events cause complex deletions and insertions at 17 sites in the mouse genome. *Nat. Commun.* **8**, 15464 (2017).
50. F. Adikusuma *et al.*, Large deletions induced by Cas9 cleavage. *Nature* **560**, E8–E9 (2018).
51. M. Kosicki, K. Tomberg, A. Bradley, Repair of double-strand breaks induced by CRISPR-Cas9 leads to large deletions and complex rearrangements. *Nat. Biotechnol.* **36**, 765–771 (2018).
52. G. Cullot *et al.*, CRISPR-Cas9 genome editing induces megabase-scale chromosomal truncations. *Nat. Commun.* **10**, 1136 (2019).
53. D. D. Owens *et al.*, Microhomologies are prevalent at Cas9-induced larger deletions. *Nucleic Acids Res.* **47**, 7402–7417 (2019).
54. M. V. Zuccaro *et al.*, Allele-specific chromosome removal after Cas9 cleavage in human embryos. *Cell* **183**, 1650–1664 (2020).
55. J. Enciso-Romero *et al.*, Evolution of novel mimicry rings facilitated by adaptive introgression in tropical butterflies. *Mol. Ecol.* **26**, 5160–5172 (2017).
56. P. Jay *et al.*, Association mapping of colour variation in a butterfly provides evidence that a supergene locks together a cluster of adaptive loci. *Philos. Trans. R Soc. B* **377**, 20210193 (2022).
57. Y. Matsuoka, A. Monteiro, Melanin pathway genes regulate color and morphology of butterfly wing scales. *Cell Rep.* **24**, 56–65 (2018).

ACKNOWLEDGMENTS. We thank T. Kirby, R. Canalichio and G. Julian for help with butterfly husbandry; S. Van Belleghem for bioinformatics assistance; the GWU HPC team for providing computing infrastructure; the GW Nanofabrication and Imaging Center (GWNIC) for microscopy resources. This work was supported by the following awards: NSF IOS-2110534 to A.M.; NSF EPSCoR OIA-1736026, PRSTRT ARG 2020-00138, and funding from the FPI at the UPR-RP to R.P. and BBSRC BB/R007500/1 to C.D.J.

Author affiliations: ^aDepartment of Biological Sciences, The George Washington University, Washington, DC 20052; ^bDepartment of Zoology, University of Cambridge, Cambridge CB2 3EJ, United Kingdom; ^cDepartment of Biology, Duke University, Durham, NC 27708; ^dSmithsonian Tropical Research Institute, Gamboa, Panama; ^eDepartment of Biology, University of Puerto Rico at Rio Piedras, San Juan 00925, Puerto Rico; ^fTree of Life, Wellcome Sanger Institute, Cambridge CB10 1RQ, United Kingdom; ^gDepartment of Ecology and Evolutionary Biology, Cornell University, Ithaca, NY 14853; ^hComprehensive Cancer Center, University of Puerto Rico, San Juan 00925, Puerto Rico; ⁱMolecular Sciences and Research Center, University of Puerto Rico, San Juan 00926, Puerto Rico; and ^jDipartimento di Scienze Chimiche della Vita e della Sostenibilità Ambientale, Università di Parma, Parma 43124, Italy

Author contributions: L.L., J.J.H., R.P., C.D.J., and A.M. designed research; L.L., J.J.H., E.E., C.J.W., L.S.L., A.M.-V., K.K., A.C., E.S.M.v.d.H., R.D.R., and A.M. performed research; L.L., J.J.H., C.J.W., and A.M.-V. analyzed data; and L.L., J.J.H., and A.M. wrote the paper.

58. R. Futahashi, M. Osanai-Futahashi, "Pigments in insects" in *Pigments, Pigment Cells and Pigment Patterns*, H. Hashimoto, M. Goda, R. Futahashi, R. Kelsh, T. Akiyama, Eds. (Springer Singapore, 2021), pp. 3-43.
59. Y. Arakane, M. Y. Noh, T. Asano, K. J. Kramer, Tyrosine metabolism for insect cuticle pigmentation and sclerotization. *Extracellular Compos. Matrices Arthropods* **40**, 165-220 (2016).
60. J. Liu *et al.*, Lepidopteran wing scales contain abundant cross-linked film-forming histidine-rich cuticular proteins. *Commun. Biol.* **4**, 491 (2021).
61. H. F. Nijhout, P. B. Koch, The distribution of radiolabeled pigment precursors in the wing patterns of nymphalid butterflies. *J. Res. Lepid.* **30**, 1-13 (1992).
62. P. B. Koch, Production of [C-14] Labeled 3-Hydroxy-L-Kynurenine in a Butterfly, *Heliconius-Charitonia L* (Heliconiidae), and Precursor Studies in Butterfly Wing Ommatins. *Pigment Cell Res.* **6**, 85-90 (1993).
63. R. D. Reed, W. O. McMillan, L. M. Nagy, Gene expression underlying adaptive variation in *Heliconius* wing patterns: Non-modular regulation of overlapping cinnabar and vermillion prepatterns. *Proc. R. Soc. B-Biol. Sci.* **275**, 37-45 (2008).
64. S. Wu *et al.*, The BTB-ZF gene Bm-mamo regulates pigmentation in silkworm caterpillars. *eLife* **12**, RP90795 (2024).
65. A. Dhir, S. Dhir, N. J. Proudfoot, C. L. Jopling, Microprocessor mediates transcriptional termination of long noncoding RNA transcripts hosting microRNAs. *Nat. Struct. Mol. Biol.* **22**, 319-327 (2015).
66. D. He *et al.*, miRNA-independent function of long noncoding pri-miRNA loci. *Proc. Natl. Acad. Sci. U.S.A.* **118**, e2017562118 (2021).
67. J. E. Collinge, A. R. Anderson, A. R. Weeks, T. K. Johnson, S. W. McKechnie, Latitudinal and cold-tolerance variation associate with DNA repeat-number variation in the hsr-omega RNA gene of *Drosophila melanogaster*. *Heredity* **101**, 260-270 (2008).
68. M. Liang *et al.*, Taxon-specific, phased siRNAs underlie a speciation locus in monkeyflowers. *Science* **379**, 576-582 (2023).
69. L. Livraghi, Dataset for "A long non-coding RNA at the cortex locus controls adaptive colouration in butterflies". Open Science Framework. <https://doi.org/10.17605/OSF.IO/Q3SY7>. Deposited 29 January 2024.
70. B. J. Haas *et al.*, De novo transcript sequence reconstruction from RNA-seq using the Trinity platform for reference generation and analysis. *Nat. Protocols* **8**, 1494-1512 (2013).
71. A. Astashyn *et al.*, Rapid and sensitive detection of genome contamination at scale with FCS-GX. *bioRxiv* [Preprint] (2023). Available at: <https://www.biorxiv.org/content/10.1101/2023.06.02.543519v1>. Accessed 3 November 2023.
72. A. C. B. Aymone, N. Lothammer, V. L. da S. Valente, A. M. de Araújo, Embryogenesis of *Heliconius erato* (Lepidoptera, Nymphalidae): A contribution to the anatomical development of an evo-devo model organism. *Dev. Growth Differ.* **56**, 448-459 (2014).
73. M. Holzem, N. Braak, O. Brattström, A. P. McGregor, C. J. Breuker, Wnt gene expression during early embryogenesis in the nymphalid butterfly *Bicyclus anynana*. *Front. Ecol. Evol.* **7**, 468 (2019).
74. J. J. Hanly *et al.*, Frizzled2 receives WntA signaling during butterfly wing pattern formation. *Development* **150**, dev201868 (2023).
75. L. Livraghi, "Sequence Read Archive (SRA) [NCBI:PRJNA1031670]". National Center for Biotechnology Information (NCBI). <https://www.ncbi.nlm.nih.gov/sra>. Deposited 24 October 2023.